Hydrogen Crossover in PEM and Alkaline Water Electrolysis: Mechanisms, Direct Comparison and Mitigation Strategies

Journal of The Electrochemical Society, **165** (7) F502-F513 (2018)
0013-4651/2018/165(7)/F502/12/$37.00 © The Electrochemical Society

Hydrogen Crossover in PEM and Alkaline Water Electrolysis: Mechanisms, Direct Comparison and Mitigation Strategies

P. Trinke,[1,=] P. Haug,[2,=] J. Brauns,[2] B. Bensmann,[1,z] R. Hanke-Rauschenbach,[1] and T. Turek[2]

[1] *Institute of Electric Power Systems, Leibniz Universität Hannover, 30167 Hanover, Germany*
[2] *Institute of Chemical and Electrochemical Process Engineering, Clausthal University of Technology, 38678 Clausthal-Zellerfeld, Germany*

This study provides a direct comparison of hydrogen crossover in PEM (Nafion 117) and alkaline water electrolysis (Zirfon) at a temperature of 60°C applying state-of-the-art separating unit materials. To this end, occurring crossover mechanisms are described first, before experimental data of the anodic hydrogen content are shown in dependence of current density, system pressure and process management strategy. The results suggest that permeation in PEM electrolyzers is mainly governed by diffusion due to a supersaturated concentration of dissolved hydrogen within the catalyst layer, showing a share of 98% of the total permeation flux at 1 A cm^{-2} and atmospheric pressure. Permeation in alkaline electrolyzers also exhibits a significant influence of supersaturation, but the overall crossover is mainly influenced by mixing the electrolyte cycles, which makes up a share of 90% at 0.7 A cm^{-2} and 1 bar. Generally it becomes evident that hydrogen permeation across the separating unit is more than one order of magnitude smaller in alkaline electrolysis, which is mainly a consequence of the significantly lower hydrogen solubility in concentrated KOH electrolyte. Finally, this study concludes with an assessment of the impact of separating unit thickness and provides mitigation strategies to reduce hydrogen crossover.
 [DOI: 10.1149/2.0541807jes]

Manuscript submitted March 14, 2018; revised manuscript received April 19, 2018. Published May 16, 2018.

Proton exchange membrane (PEM) and alkaline water electrolysis (AEL) represent two promising technologies, which are capable of the future production of renewable hydrogen. It has already been demonstrated that both technologies can react quickly to dynamic power profiles from renewable energy sources.[1,2] Generally, both electrolysis technologies are operated in a similar range of parameters to split water into the constituents hydrogen and oxygen (Eq. 1). Thus, temperatures between 50 and 80°C or system pressures up to 30 bar represent the current state of the art.[3]

$$H_2O \longrightarrow H_2 + 0.5O_2 \quad [1]$$

The main difference between these two technologies lies in the application of either an acid or alkaline electrolyte. In PEM electrolysis protons are used for the charge transport as it is shown in the anodic and cathodic half cell reactions (Eqs. 2 and 3).

$$\text{Anode:} \quad H_2O \longrightarrow 2H^+ + 0.5O_2 + 2e^- \quad [2]$$

$$\text{Cathode:} \quad 2H^+ + 2e^- \longrightarrow H_2 \quad [3]$$

On the contrary, hydroxide ions are responsible for the charge exchange in AEL (Eqs. 4 and 5).

$$\text{Anode:} \quad 2OH^- \longrightarrow 0.5O_2 + H_2O + 2e^- \quad [4]$$

$$\text{Cathode:} \quad 2H_2O + 2e^- \longrightarrow H_2 + 2OH^- \quad [5]$$

However, both technologies face similar issues, which need to be solved for a successful coupling with renewable energy sources. Thus, gas crossover represents one of the main issues in PEM and alkaline water electrolysis so far. Especially the permeation of hydrogen into the anodic half cell is of special importance, as explosive gas mixtures can form in the part-load operation range of the electrolyzers, e.g. Refs. 4–7. However, this problem can be solved relatively easily by the application of recombination catalysts as it has already been demonstrated for PEM electrolysis. Grigoriev et al.[8] showed that the anodic hydrogen content could be significantly reduced using a recombination catalyst, which was applied at the back side of the porous transport layer (PTL). A further improvement of the anodic gas purity could be achieved when the recombination catalyst was placed in the product gas conduits downstream of the gas separators. Another possibility is the utilization of electrocatalysts, which also promote the oxidation of hydrogen and recombination with evolved oxygen to water. Ito et al.[9] reported a decrease of the measured hydrogen fraction if a platinum based reversed catalyst coated membrane (CCM) was used for fuel cell and electrolysis operation. However, it is important to emphasize that recombination catalysts only reduce the risk of safety issues, but do not address the origin of crossover directly. Two further negative side effects of gas crossover, degradation[10,11] and reduction of Faraday efficiency,[8,12] are still present. However, especially degradation, which has been observed in PEM electrolysis, should not be neglected as the trend toward thinner membranes may further enhance gas crossover. So far, for AEL no publication could be found that establishes a link between gas crossover and electrode degradation, although this dependency also could exist. Nevertheless, the safety problem still represents a major issue in AEL.

Most recent publications on gas crossover in PEM electrolysis are focused on the investigation of the current density influence. It could be shown so far that hydrogen and oxygen crossover increases linearly with the applied current density.[5,13,14] The publications on AEL in contrast are mostly focused on the influence of separator and membrane materials, as well as process conditions on the anodic hydrogen fractions. Furthermore, strategies are provided, which may be used for an improved anodic gas purity.[7,15,16]

The present contribution firstly provides a summary on the occurring crossover mechanisms in PEM and alkaline water electrolysis. Subsequently, experimental data of the influence of current density, system pressure and various process management possibilities on the anodic hydrogen content is shown for both electrolysis technologies. In order to create comparable crossover data, the experiments of both technologies are carried out with state-of-the-art separating unit materials (PEM: Nafion 117, AEL: Zirfon) and at identical process temperatures. The obtained results are then used to identify the most influential crossover mechanism in PEM and alkaline electrolysis. Finally, the study provides an estimation of the influence of separating unit thickness on hydrogen crossover and makes proposals on possible crossover mitigation strategies.

Experimental Setup and Method

Cell design.—*PEM electrolysis.*—The PEM water electrolysis experiments in this study were conducted with a commercially available electrolysis cell (Sylatech Analysetechnik GmbH, type ZE 200), which is shown in Fig. 1a. The cell has a circular design with an active area of 62 cm^2 without flow field structures. On the anode side a titanium mesh serves as a water distributor. Between the mesh and the CCM a PTL is incorporated, which consists of sintered titanium

[=]These authors contributed equally to this work.
[z]E-mail: boris.bensmann@ifes.uni-hannover.de

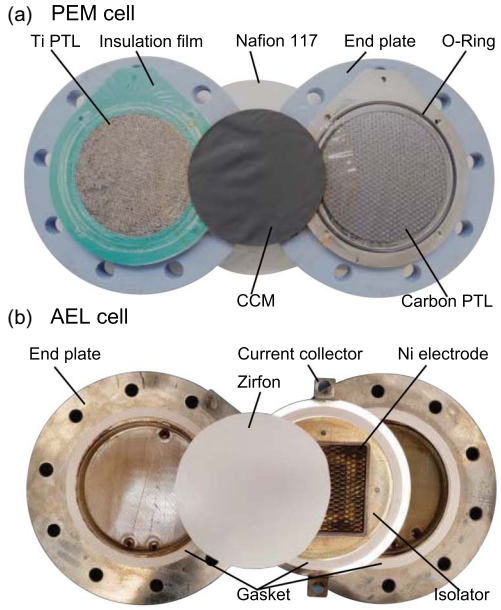

Figure 1. Cell designs of the applied PEM (a) and alkaline (b) electrolysis cells (pictures are not scaled).

fibers. In the cathodic half cell a porous graphite plate is implemented, whereas an O-ring is used for sealing of the electrolysis cell. The CCM is based on a Nafion 117 membrane, which was manufactured by HIAT gGmbH with anode and cathode catalyst loadings of 2 $mg_{Ir}\,cm^{-2}$ and 1 $mg_{Pt}\,cm^{-2}$, respectively. The dry Nafion membrane has a thickness of approximately 180 µm, the porosity amounts to $\varepsilon = 0.37$ (water volume) and the channel diameter is roughly $d = 2.5$ nm.[a,17] The whole cell was encased with thermal insulating fabric for isothermal operating conditions.

Alkaline electrolysis.—The AEL experiments were conducted with a custom-built single electrolysis cell, which consists of two end plates, current collectors, electrode mounts, electrodes and a separator for keeping the product gases apart. Fig. 1b depicts a choice of these cell components. The end plates are made of nickel coated 304 steel and are used for the electrolyte supply and removal. Additionally, each end plate provides a circular electrolyte volume of roughly 300 mL. The electrolysis voltage can be applied through current collectors out of 316Ti steel, which are connected to the electrode mounts via bolted connections.

The active electrodes themselves consist of quadratic Nickel (Alloy 201) expanded metal with a geometrical area of 100 cm^2 and are welded on the electrode mounts of the same material. These electrodes are directly pressed onto a circular Zirfon Perl UTP 500 separator with a geometrical area of 227 cm^2, so that a zero-gap cell arrangement is achieved. The manufacturer AGFA specifies the separator thickness with $\delta_{sep} = 500 \pm 50$ µm, the separator porosity with $\varepsilon = 0.5 \pm 0.1$ and the pore diameter with $d = 150 \pm 50$ nm.[18] Furthermore the cell contains 3D-printed polypropylene inlays, which are necessary for the electrical insulation of the current collectors from other cell components.

Test station.—*PEM electrolysis.*—A Greenlight test station (E100) supplies the anodic compartment of the PEM electrolysis cell with 150 ± 5 mg min^{-1} deionized water at a temperature of 60°C. The galvanostatic steps are applied by an Ametek Sorensen XG 6-220 power supply with an accuracy of ± 0.2% of the output current reading. The flow sheet of the test station is shown in Fig. 2a. On each side the gas-water mixture is separated by two gas separators and an intermediate cooling step of the gas after the outlet of the first separator. The water of the anode is cycled, whereas on the cathode the separated water is drained.

Pressure control valves regulate the absolute cathodic gas pressure to 1, 10 and 20 bar, whereas on the anode side pressures of 1 and 10 bar are applied. The error of this regulation is less than ± 0.2 bar. Every three minutes a micro-GC (Agilent 490) takes a gas sample of the anodic product gas to measure the concentration of hydrogen in oxygen. This micro-GC is equipped with a 10 m long 5Å molesieve column and a thermal conductivity detector for permanent gas separation and detection. Test gas mixtures with hydrogen concentrations of 0.1, 1 and 2.5 vol.% in oxygen (accuracy of reading ± 2%, Linde) were used for calibration of the GC. The calibration measurements indicated a standard deviation of ± 0.006 vol.%. Furthermore, it is possible to directly feed the electrolysis cell with oxygen (Linde 5.0) and hydrogen (Linde 5.0) to the corresponding cell inlet with an accuracy of ± 1% of the reading. This gas feed is mandatory for reference measurements, which will be described later in this study.

Alkaline electrolysis.—The alkaline test cell was connected to a Greenlight test station (E40), which continuously supplies the anodic and cathodic half cell with a 32 wt% KOH electrolyte solution at a flow rate of 0.350 ± 0.002 L min^{-1}, a temperature of 60°C and absolute system pressures of 1, 10 and 20 bar. Here, both half cell compartments are always operated at equalized pressure. With the given volumetric flow rate, the electrolyte of each half cell is replaced 70 times per hour, which is defined as the recirculation rate within this work. The electrolysis power is supplied by an Ametek Sorensen XG 12–140 power supply, which is used for galvanostatic measurements with an accuracy of ± 0.2% of the rated output current.

Downstream of the electrolysis cell the gas-liquid mixtures are fed to gas separators, where the evolved gaseous products are removed from the electrolyte solution. The rising gas flows are then cooled down to approximately 25°C to reduce the water content of the product gases. The condensed water is collected in a tank and fed back into the gas separators. The remaining gaseous water content is then further reduced by desiccant dryers, before the composition of the product gas streams is analyzed in an online gas chromatograph (Agilent 7820A) every 5 minutes, which is also equipped with a molesieve column and a thermal conductivity detector. Calibration of the GC was carried out with test gas compositions of 0.02, 0.2 and 1 vol.% hydrogen in argon, which could be determined with a maximum error of ± 0.01 vol.%. The liquid electrolyte from the gas separators, however, is led back to the mixing point of the electrolyte cycles in order to compensate the concentration difference caused by the electrode reactions (Eqs. 4 and 5). Besides the classical electrolyzer operation with mixed electrolyte cycles, this test station also possesses the possibility to separate the cycles by changing the valve position of the 3/2-way valves, which are shown in the flow sheet in Fig. 2b. It can further be seen in the flow sheet that it is possible to feed the cell via Bronkhorst mass flow controllers with hydrogen (Linde 5.0) to the cathodic and oxygen (Linde 3.5) to the anodic half cell with an accuracy of ± 0.5% of the desired setpoint.

Methods.—*In this study the stationary anodic hydrogen contents at a fixed temperature of 60°C, absolute pressures of 1, 10 and 20 bar and various current densities in the range of 0.05 to 0.9 A cm^{-2} were determined by online gas chromatography for PEM and alkaline water electrolysis. In both experimental setups stationary data was achieved in such way that a specific current density was applied to the electrolysis cell and chromatograms were recorded simultaneously. The current density was kept constant until the measured hydrogen fraction remained unchanged for at least 1 h before it was changed to the next operating point. For determination of the hydrogen content with separated electrolyte cycles in AEL, the cycles were remixed after each operating point to account for the arisen electrolyte concentration difference.*

[a]porosity and diameter were measured for a Nafion 115 membrane

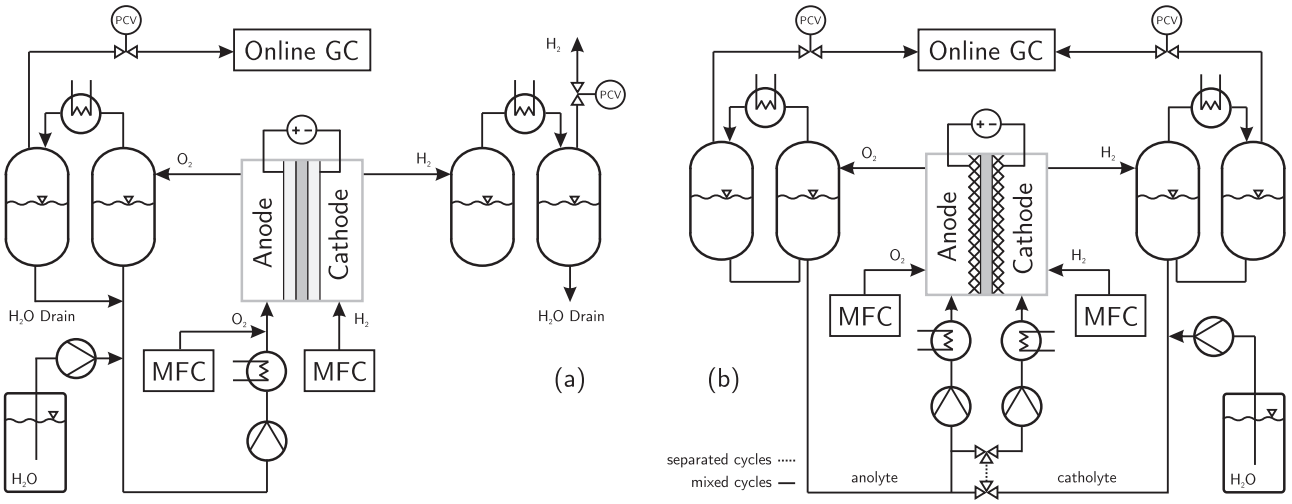

Figure 2. Schematic flow sheets of the PEM (a) and AEL (b) test stations applied in this study.

Similarly, experiments were carried out in which the PEM and alkaline electrolysis cells were disconnected from the power supply, but fed with hydrogen and oxygen according to their volumetric flow rates representing a current density range from 0.05 to 0.9 A cm^{-2}. In the following these experiments are referred to as reference measurements, which have only been conducted at atmospheric pressure and 60°C.

With the experimental data from the electrolysis and reference measurements it is possible to derive the hydrogen permeation rate through the membrane or separator while presuming that the anodic catalyst materials are inactive for the oxidation of hydrogen. Thus, all the permeating hydrogen can be measured in the anodic product gas stream. For the AEL this is only valid for experiments with separated electrolyte cycles. Additionally, it has to be assumed that the oxygen permeation rate is negligibly small compared to the evolution rate of oxygen. This assumption can be made for PEM electrolysis as the oxygen permeation through a Nafion membrane is reported to be at least two times smaller than its hydrogen counterpart.[19] For AEL this assumption is also admissible as the hydrogen diffusion coefficient in 32 wt% KOH at 60°C is about three times larger than that of oxygen.[20] The measured water-free anodic hydrogen fraction Φ_{H_2} can then be described according to Eq. 6.

$$\Phi_{H_2} = \frac{N_{H_2}^{perm}}{N_{O_2}^{ano} + N_{H_2}^{perm}} \quad [6]$$

Within Eq. 6 $N_{H_2}^{perm}$ denotes the hydrogen permeation flux, whereas the anodically evolving oxygen flux is represented by $N_{O_2}^{ano}$. This oxygen flux in turn can be obtained by insertion of the applied current density i into Faraday's law (Eq. 7) for the anodic half cell reaction.

$$N_{O_2}^{ano} = \frac{i}{4F} \quad [7]$$

With these two equations it is now possible to derive the hydrogen permeation flux from the experimentally determined anodic hydrogen content. Therefore, Eq. 7 needs to be inserted into Eq. 6 and solved for the hydrogen permeation flux $N_{H_2}^{perm}$.

$$N_{H_2}^{perm} = \frac{i}{4F} \frac{\Phi_{H_2}}{1 - \Phi_{H_2}} \quad [8]$$

It has to be kept in mind that this equation is only valid if the separating unit surface area equals the geometrical area of the electrodes. Otherwise Eq. 8 needs to be multiplied by the ratio of electrode and separating unit area to account for the additional permeation area (Eq. 9).

$$N_{H_2}^{perm} = \frac{i}{4F} \frac{\Phi_{H_2}}{1 - \Phi_{H_2}} \frac{A_{el}}{A_{sep}} \quad [9]$$

Pressure drop method.—For the PEM setup further crossover measurements were conducted with the so called pressure drop method. Therefore, the cathode is pumped up with hydrogen gas. After reaching the targeted pressure, a valve on the cathode side is closed. The pressure drop is recorded by a pressure sensor (P-30: 0–40 bar, Wika). The gas leakage rate of the applied cell was negligibly low in comparison to the crossover. Consequently, the measured pressure decreasing rate is proportional to the hydrogen crossover that can be calculated by the cathodic mass balance. This method can be classified as a dynamical pressure measurement with a constant volume.[21]

Crossover Mechanisms

For both electrolysis technologies several possibilities exist, which cause hydrogen crossover. In general these permeation routes can be divided into diffusive and convective mass transfer mechanisms. This chapter will give an overview on the occurring mass transfer mechanisms and will rather point out, which of them are technology specific.

Diffusion.—One of the possible crossover mechanisms is the diffusion of electrolysis products across the membrane or separator into the opposite half cell compartment for both technologies. Generally, the products may diffuse through the solid and aqueous phase of the separating unit. However, it is reported that diffusion through the solid phase of a fully hydrated Nafion membrane is roughly one order of magnitude smaller compared to its liquid phase.[22,23] Similar information can be found for Zirfon as the diffusion through the separator's solid phase is also assumed to be negligible. Additionally, the separator is further presumed to be impermeable for gas bubbles at atmospheric pressure.[24] Thus, it is comprehensible for both technologies that only species that are dissolved in water or KOH solution are considered for diffusion across the separating unit. This is typically done by application of Fick's law (Eq. 10) in PEM[4,25–28] and alkaline water electrolysis:[16]

$$N_{H_2}^{diff} = D_{H_2}^{eff} \frac{\Delta c_{H_2}}{\delta_{sep}} \quad [10]$$

Here, Δc_{H_2} represents the dissolved hydrogen concentration gradient across the separating unit with the thickness δ_{sep}, whereas $D_{H_2}^{eff}$ denotes the effective diffusion coefficient of hydrogen in the membrane

or separator. The estimation of the effective diffusion coefficient in polymer electrolyte membranes[29] or porous media[30] is typically done by correction of the molecular diffusion coefficient in the aqueous solvent D_{H_2} with the porosity ε and tortuosity τ of the separating unit (Eq. 11).

$$D_{H_2}^{eff} = \frac{\varepsilon}{\tau} D_{H_2} \quad [11]$$

In PEM electrolysis the concentration gradient across the membrane Δc_{H_2} can be estimated with the cathodic concentration of dissolved hydrogen $c_{H_2}^{cat}$ as the anodic hydrogen concentration $c_{H_2}^{ano}$ is approximately zero. However, this assumption becomes also applicable for AEL if the electrolyzer is operated with separated electrolyte cycles.

$$\Delta c_{H_2} \approx c_{H_2}^{cat} - \cancelto{0}{c_{H_2}^{ano}} \quad [12]$$

Henry's law (Eq. 13) states that a species' dissolved concentration is directly proportional to its partial pressure in the gas phase. Therefore, this approach can be applied for the calculation of the cathodic dissolved hydrogen concentration. Within the following Eq. 13 S_{H_2} denotes the hydrogen solubility in the solvent, whereas the cathodic hydrogen partial pressure is represented by $p_{H_2}^{cat}$.

$$c_{H_2}^{cat} = S_{H_2} p_{H_2}^{cat} \quad [13]$$

Data of the hydrogen solubility in pure water was published by Young et al.[31] for atmospheric pressure conditions. Further data for pressures ranging from 25 to 1000 atm can be found in the publication by Wiebe and Gaddy.[32] However, literature for the hydrogen solubility in concentrated potassium hydroxide solution is scarce. Ruetschi and Amlie[33] reported data for various electrolyte concentrations at a temperature of 30°C and atmospheric pressure, whereas Knaster and Apel'baum[34] provided further values at temperatures of 21, 45 and 75°C.

The cathodic hydrogen partial pressure can be obtained if it is assumed that the cathodic oxygen partial pressure is negligible and that the hydrogen is saturated with water vapor. Then the following Eq. 14 applies, where p^{cat} denotes the total cathodic pressure:

$$p_{H_2}^{cat} = p^{cat} - p_{H_2O}^{cat} \quad [14]$$

The calculation of the water vapor pressure may be performed by application of the Antoine equation with parameters for pure water, e.g. Ref. 35. However, the estimation of the water vapor pressure above a potassium hydroxide solution necessitates the empirical correlations by Balej.[36]

Finally, the diffusional hydrogen flux across the separating unit can be described with the following Eq. 15 if the aforementioned assumptions apply and Eq. 13 is inserted into Eq. 10.

$$N_{H_2}^{diff} = D_{H_2}^{eff} S_{H_2} \frac{p_{H_2}^{cat}}{\delta_{sep}} \quad [15]$$

The product of the effective diffusion and solubility coefficient $D_{H_2}^{eff} S_{H_2}$ is frequently provided in form of the permeability coefficient K_{H_2}, which is a classical material property for separating units.

Convection.—Convection represents another general cause of crossover, which can be divided into several further mechanisms. Generally, convective mass transport is mathematically expressed by Eq. 16. There, v_{solv} describes the velocity of solvent (PEM: water, AEL: KOH solution) moving perpendicular to the separating unit, whereas c_{H_2} denotes the concentration of dissolved gas within the solvent.

$$N_{H_2}^{conv} = v_{solv} c_{H_2} \quad [16]$$

Differential pressure.—One possible reason for convective permeation is the transport of electrolyte and dissolved species across the separating unit due to the presence of total pressure gradients. For the mathematical description of this transport mechanism commonly Darcy's law (Eq. 17) is applied, e.g. Refs. 24, 25, 28 and 37.

$$N_{H_2}^{dp} = \frac{K_{sep}}{\eta} S_{H_2} p_{H_2}^{cat} \frac{\Delta p}{\delta_{sep}} \quad [17]$$

Here, K_{sep} denotes the permeability of the separating unit, η is the dynamic viscosity of the solvent, whereas Δp describes the absolute pressure difference between the cathodic and anodic compartment. The concentration of dissolved hydrogen is again estimated by the insertion of Henry's law (Eq. 13). The hydraulic permeability K_{sep} of porous media such as membranes can be estimated by the Hagen-Poiseuille (Eq. 18) or Kozeny-Carman (Eq. 19) equations.[38]

$$K_{sep} = \frac{\varepsilon d^2}{32\tau} \quad [18]$$

$$K_{sep} = \frac{\varepsilon^3}{K_{koz} a^2 (1-\varepsilon)^2} \quad [19]$$

Here, ε represents the porosity, d the pore diameter, τ the tortuosity and a the specific surface area of the separating unit, while K_{koz} denotes the Kozeny constant, which depends on the porous media.[39] For a rough estimation of the hydraulic permeability K_{sep} in this work the Hagen-Poiseuille equation (Eq. 18) is used. The necessary porosities and pore diameters of both applied separating units are given within the setup section. In order to make a worst case estimate the tortuosity is chosen to be $\tau = 1.5$ for both systems. Therewith the permeability for the Nafion membrane and Zirfon separator are approximated to be $5 \cdot 10^{-20}$ m^2 and $2 \cdot 10^{-16}$ m^2, respectively. These estimates match literature data of both separating units quite well, e.g. Refs. 17 and 40. Hence, AEL with a porous separator is theoretically more prone to convective permeation. But it has to be noted that it is also more convenient to mix the electrolyte cycles at identical pressure levels, which is also an important reason for balanced pressure operation. However, if it is assumed that commonly applied back pressure control valves are capable of controlling the anodic and cathodic pressures with an accuracy of roughly 1%, it becomes comprehensible that a differential pressure across the separator may be formed. Thus, it is conceivable that either dissolved hydrogen or oxygen could convectively be transported into the opposite half cell.

In contrast, literature suggests that no pressure-driven permeation is evident for Nafion membranes,[23,41] which is supported by the low calculated permeability of the membrane used in this study. This allows the operation of PEM electrolyzers under asymmetrical pressure conditions. Here, the cathode is typically pressurized, whereas the anodic cycle stays at atmospheric pressure, which can be favorable in terms of energy demand, e.g. Refs. 26, 42, and 43. However, if alternative membrane materials are applied, this operation mode may also promote a permeation flux as the resulting pressure-driven water flow carries dissolved hydrogen into the anodic compartment.[28]

Electro-osmostic drag.—A further possibility to cause convective permeation is the electro-osmotic drag. Due to the electric field and the associated movement of ions, the electroneutral solvent can be dragged with them across the separating unit. Hence, dissolved gas may also be transported through it.[26,28,44] Thus, in PEM electrolysis dissolved oxygen may be dragged along with the transport of protons from the anodic into the cathodic half cell. In contrast, the electro-osmotic drag could also be capable of reducing hydrogen permeation as it may transport dissolved hydrogen back to the cathode. On the contrary, OH^- ions are responsible for the charge transport in AEL. According to the half cell reactions (Eqs. 4 and 5) these hydroxide ions are transported from the cathodic to the anodic compartment, which therefore may enhance hydrogen and reduce oxygen crossover. However, no publication was found that could confirm or quantify this mechanism. A rough estimation of the electro-osmotic crossover flux can be carried out with the following Eq. 20:

$$N_{H_2}^{drag} = \frac{S_{H_2} p_{H_2}^{cat}}{c_{solv}} \frac{n_{drag} i}{F} \quad [20]$$

Here, c_{solv} is the concentration of solvent within the separating unit and n_{drag} is the electro-osmotic drag coefficient, which describes the ratio between the flux of dragged solvent molecules to that of the charged ions. Jacobson et al.[45] compared drag coefficients of proton-conducting Nafion membranes to that of a hydroxide-conducting Tokuyama A201 membrane for the application in acid and alkaline fuel cells. Their results showed a smaller value for the anion-conducting membrane, which may be attributed to the different charge carrier or water domain. A temperature-dependent correlation for the estimation of the drag coefficient in a Nafion membrane used for PEM electrolysis can be found in the publication by Onda et al.[46]

Electrolyte mixing.—The electrochemical reactions in AEL (Eqs. 4 and 5) cause a change in electrolyte concentration since water is consumed at the cathode, whereas it is produced in the anodic half cell. Therefore, the anodic and cathodic electrolyte cycles are usually mixed together to balance this concentration gradient.[47] However, this process management leads to a decrease of the resulting product gas purity as the electrolyte is saturated with dissolved electrolysis products. Thus, the electrolysis cell is continuously fed with dissolved hydrogen and oxygen from the gas separators, where they are then able to outgas. Of course, separating the electrolyte cycles prevents this crossover mechanism at all. But due to the shift in the anodic and cathodic electrolyte concentrations the cell efficiency may decrease, as the electrolyte conductivity is reduced with prolonged time.

Supersaturation.—It is generally assumed for gas evolving electrodes that the electrolysis products are produced in dissolved form[48] before gas bubbles grow at active nucleation sites. Nucleation sites are small electrode surface irregularities, which depend on the material and its roughness.[49] For the nucleation sites to become active a sufficient deviation from equilibrium concentration of the generated product is mandatory.[50] Therefore, the electrolyte becomes supersaturated, which describes a higher concentration of dissolved hydrogen within the electrode boundary or catalyst layer than it would be expected through Henry's law (Eq. 13). The existence of this supersaturated concentration of dissolved species could already be proven experimentally, e.g. Refs. 51 and 52. Consequently, the subsequent mass transfer of dissolved hydrogen is mainly controlled by two competing mechanisms. Thus, dissolved hydrogen is either transported to the electrolyte bulk in dissolved form or to the gas-liquid interface of gas bubbles present in the electrode boundary layer.[53] However, dissolved hydrogen may also be transported through the separating unit of the electrolysis cell.[5]

As theory of the aforementioned diffusive and convective crossover mechanisms only supposed hydrogen equilibrium concentration (Henry's law), supersaturation enhances these crossover mechanisms in PEM and zero-gap alkaline electrolysis. However, the influence of supersaturation on crossover can only be accounted, if the previously mentioned equations are expressed in their concentration forms instead of the gas pressure expressions. Then Eq. 21 can be used for the calculation of the dissolved gas concentration within the catalyst layer in PEM electrolysis:[5]

$$c_{H_2}^{cat} = \frac{\frac{i}{2F} + k_L p_{H_2}^{cat} S_{H_2}}{k_L + \frac{D_{H_2}^{eff}}{\delta_{sep}}} \quad [21]$$

Here k_L denotes the mass transfer coefficient, which includes several transport and transfer steps: beginning with the desorption of the electrolysis product from the catalyst particles up to the transfer into the gas phase within the pore space. For the PEM catalyst layers it is suggested that this mass transfer coefficient is significantly affected by the diffusion of the dissolved gas from the catalyst particles to the pore space through the ionomer. Already small limitations can lead to a significant increase of the dissolved gas concentration.[5] Additionally, Eq. 21 reveals that supersaturation also increases toward higher current densities. So, it is necessary to consider that the concentration of dissolved gas is not solely a function of gas solubility, system pressure and the electrode specific mass transfer coefficient, but also of current density: $c_{H_2}^{cat} = f(p_{H_2}^{cat}, S_{H_2}, k_L, i)$.

Summary and comparison of crossover mechanisms.—The previously described crossover mechanisms of both technologies are summarized and directly compared in Table I. It is stated, which impact each individual crossover mechanism has on the overall crossover flux of the respective technology. The assessment of the individual influences is supported by a direct comparison of the key parameters controlling the mechanisms. Therefore, the crossover equations are given in their concentration forms.

For diffusive crossover through the separating unit every relevant parameter effects a higher permeation rate for PEM electrolysis

Table I. Comparison of the crossover mechanisms with key parameters and evaluation of the impact on the overall gas crossover of the respective technology. If no special information given, stated values are valid for a temperature of 60°C and in case of AEL for a KOH concentration of 30 wt%.

Mechanism	Equation: Parameter/Symbol/Unit	PEM (Nafion)		AEL (Zirfon)
Diffusion	$N_{H_2}^{diff} = D_{H_2}^{eff} \frac{c_{H_2}^{cat}(p_{H_2}^{cat}, S_{H_2}, k_L, i)}{\delta_{sep}}$	very high	$\gg$	low
	thickness/δ_{sep}/µm	20–250	$<$	500
	solubility coeff./S_{H_2}/mol Pa^{-1} m^{-3}	3.8e-6[a,33]	$\gg$	3.6e-7[b,33]
	diff. coeff. in solvent/D_{H_2}/m^2 s^{-1}	8.9e-9[c,54]	$>$	3.3e-9[c,20]
Convective				
Differential pressure	$N_{H_2}^{dp} = \frac{K_{sep}}{\eta} c_{H_2}^{cat}(p_{H_2}^{cat}, S_{H_2}, k_L, i) \frac{\Delta p}{\delta_{sep}}$	low	$\ll$	possibly high
	hydr. permeability/K_{sep}/m^2	5e-20[d]	$\ll$	2e-16[d]
Electro-osmotic drag	$N_{H_2}^{drag} = \frac{c_{H_2}^{cat}(p_{H_2}^{cat}, S_{H_2}, k_L, i)}{c_{solv}} \frac{n_{drag} i}{F}$	low[e]	$>$	even lower[e]
	drag coeff./n_{drag}/–	2.8[45]–4.5[46]	$>$	1.3[f,45]
	solvent conc./c_{solv}/mol m^{-3}	55e3[g]	$\approx$	56e3[g]
Electrolyte mixing	$N_{H_2}^{mix} = f(p_{H_2}^{cat}, S_{H_2}, k_L, i, \dot{V})$	no mixing	$\ll$	very high

[a] value for 30°C in pure water.
[b] value for 30°C in 32.3 wt% KOH.
[c] diff. coeff. for water and 30 wt% KOH – the eff. coeff. can be estimated via Eq. 11.
[d] calculated within this work via Eq. 18.
[e] absolute convective drag may be lower for AEL, but due to opposite ion migration hydrogen permeation is increased in AEL and decreased in PEM.
[f] value for a Tokuyama A201 anion exchange membrane.
[g] estimated by the following equation: $c_{solv} \approx \frac{\varrho_{solv}}{M_{solv}}$.

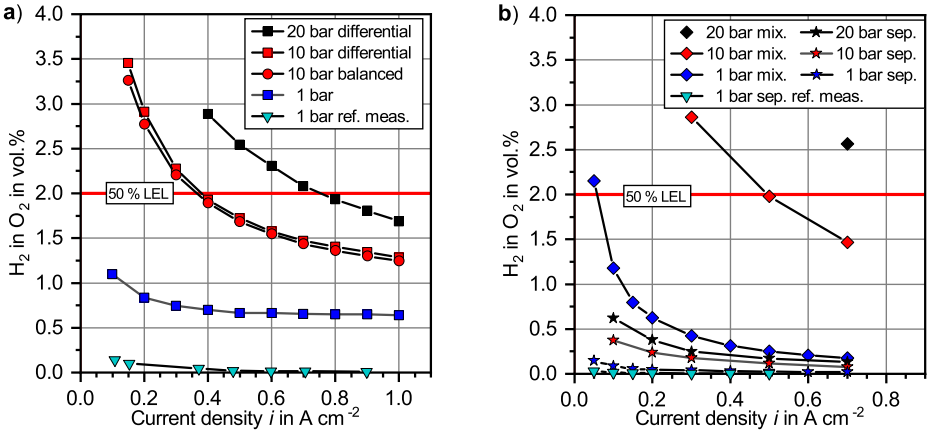

Figure 3. Measured anodic hydrogen content as a function of current density for the PEM (a) and alkaline (b) electrolysis setup at a temperature of 60°C, different system pressures and process management strategies.

compared to alkaline cells. The membrane is thinner and the diffusion coefficient of hydrogen in pure water is larger than in a KOH solution. Certainly, the solubility of hydrogen in pure water is also one order of magnitude higher than in a 30 wt% KOH electrolyte. For lower concentrations of KOH the diffusion and solubility coefficients increase toward the values of water. Consequently, the diffusive crossover increases in AEL with lower concentrated potassium hydroxide electrolytes.

The convective crossover is divided into the three different mechanisms: differential pressure, electro-osmotic drag and electrolyte mixing. As it was discussed previously, dissolved hydrogen can be carried into the anodic half cell due to a pressure-driven water or electrolyte flow. Therefore, low hydraulic permeabilities are essential to avoid this crossover mechanism. In this case, the Zirfon separator applied in AEL shows a 3 to 4 orders of magnitude higher hydraulic permeability than the Nafion membrane. Although hydrogen solubility in concentrated alkaline electrolytes is low, the estimated permeability of the Zirfon separator allows a distinct crossover at moderate pressure gradients already.

In contrast, the second convective crossover through the separating unit caused by the electro-osmotic drag is higher for PEM electrolysis as the water drag coefficient and solubility is larger in this case. However, the electro-osmotic drag is assumed to reduce hydrogen, but increase oxygen crossover in PEM electrolysis. This is different for AEL as the ions migrate into opposite directions in the two technologies. Nevertheless, the influence of this crossover mechanism is assumed to be small, since the estimation only suggests a small flow of dragged water or electrolyte with low concentrations of dissolved gas. However, at high current densities and high system pressures this mechanism can become more important as the concentration of dissolved gas is increased.

Since mixing of the anodic and cathodic electrolyte cycles is not performed in PEM electrolysis, this represents no crossover mechanism here. In contrast, this is one of the main sources of crossover in AEL. The mixing of gas saturated electrolyte cycles leads to a high exchange of both gases. This phenomenon is mainly influenced by the dissolved gas concentrations and the electrolyte flow rates, but also by the applied gas separators. Consequently no single equation can be used to calculate hydrogen crossover through electrolyte mixing. Nevertheless, a mathematical model was presented in a previous publication,[16] which can be used for an estimation of this crossover effect.

Results and Discussion

Firstly, this section illustrates the influence of current density and system pressure on the measured gas purity in PEM and alkaline electrolysis. Subsequently, the permeation fluxes through the separating units are derived from these experimental results in order to clarify the influence of current density. Following this, a breakdown of the individual crossover mechanisms of both technologies is shown. Finally, the chapter is concluded by a study of the influence of the separating unit thickness on the anodic hydrogen content.

Anodic hydrogen impurity.—Figs. 3a and 3b summarize the measured anodic hydrogen fractions of the experiments conducted in this work for a current density range from 0.05 to 1 A cm^{-2}, pressures ranging from 1 to 20 bar, a temperature of 60°C and different process management possibilities. Additionally, the results of the reference measurements without electrolysis operation are shown.

Firstly, it becomes obvious for both electrolysis technologies that higher applied current densities lead to a decrease of the anodic hydrogen contamination. This can be explained with a rising oxygen evolution rate $N_{O_2}^{ano}$ toward higher current densities, which dilutes the permeating hydrogen and therefore reduces its fraction (s. Eqs. 6 and 7).

It can further be seen in both experimental data sets that an increase of the operating pressure effects a drastic increase of the anodic hydrogen content. Thus, in PEM electrolysis a pressure change from 1 to 20 bar leads to an increase of the anodic hydrogen content from 0.654 to 2.08 vol.% at a current density of 0.7 A cm^{-2}. Accordingly, in AEL equal operating conditions caused an increase from 0.018 to 0.130 vol.% with separated electrolyte cycles, whereas mixed cycles yielded a change from 0.178 to 2.564 vol.%. So, it becomes clear that alkaline process management possibilities reveal distinct differences in the resulting anodic hydrogen fraction. This huge deviation is caused by the mixing of the anodic and cathodic electrolyte cycles. Thus, depending on the separation performance of the gas separators, dissolved or even gaseous hydrogen is transported into the anodic half cell where it contaminates the evolving oxygen. This effect becomes more relevant toward rising system pressures as the amount of dissolved gas within the electrolyte increases, whereas the mean gas bubble diameter decreases, which further complicates a proper gas separation. However, it has to be stated that hydrogen crossover due to electrolyte cycle mixing becomes less important with a growing electrolysis plant size if the electrolyte recirculation rate is kept constant.[7,55] The alkaline electrolyzer in this study was operated with a recirculation rate of 70 electrolyte replacements an hour. For minimum crossover through electrolyte mixing, the recirculation rate should always be kept as low as possible. It must be ensured though that the flow rate is high enough to keep the temperature increase within the cell below certain limits. Furthermore, it is important to emphasize that a reduction of the electrolyte recirculation may lead to an increase of the electrode bubble coverage, which effects an increase of cell voltage. In PEM electrolysis, by contrast, no significant distinction between differential and balanced pressure operation is noticeable at a system or cathodic pressure of 10 bar.

As it was described earlier, both electrolysis test cells were also fed with hydrogen and oxygen according to their volumetric flow rates in a current density range from 0.05 to 0.9 A cm^{-2} while being

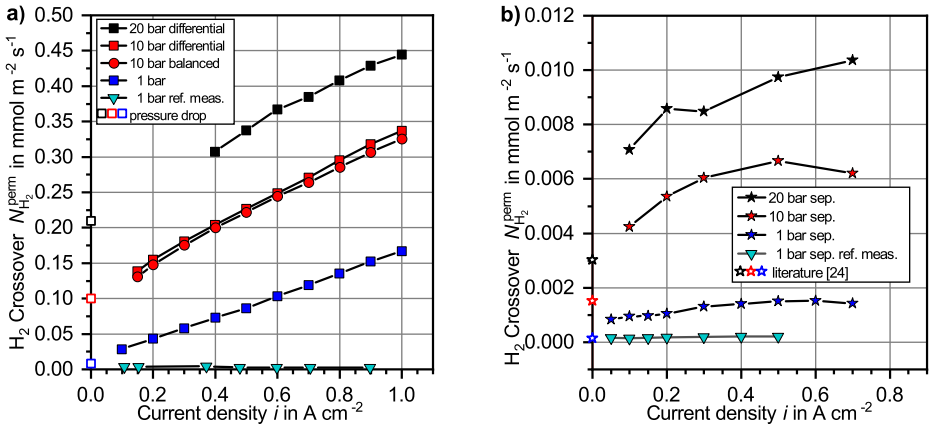

Figure 4. Determined hydrogen crossover in the PEM (a) and alkaline (b) electrolysis setup at different pressure conditions and 60°C. Hollow symbols at the y-axis represent pressure drop and literature data.

disconnected from the power supply. In the following, these experiments will be referred to as reference measurements. The obtained results are also included in Fig. 3. It can easily be seen that the measured hydrogen fractions are well below the results of the electrolysis measurements. While only a value of 0.022 vol.% was measured in the PEM setup, the alkaline cell yielded a concentration of 0.004 vol.% with separated electrolyte cycles at a current density of 0.5 A cm^{-2}.

In summary, the results indicate clearly that safety issues limit the pressurized operation of the PEM and classical alkaline electrolysis setup with mixed electrolyte cycles as the anodic hydrogen content rises above 2 vol.%, which corresponds to approximately 50% of the lower explosion limit.[47] Consequently, electrolyzers are typically shut down as soon as this concentration is exceeded.[1,6] Therefore, both electrolysis test stations cannot be operated safely under specific current density and pressure conditions if no measures are taken to reduce the crossover or the hydrogen content within the anodic half cell. Subsequently to this chapter different mitigation strategies are discussed.

Hydrogen permeation through the separating unit.—With the previously shown hydrogen fractions it is hard to assess the correlation between hydrogen crossover and current density. However, with Eq. 8 or Eq. 9 and the measured hydrogen content, the hydrogen crossover $N_{H_2}^{perm}$ can be achieved for the different applied current densities. In Figs. 4a and 4b the determined hydrogen crossover through the Nafion 117 membrane and the Zirfon separator is shown as a function of current density. In case of the alkaline system, measurement data with mixed electrolyte cycles are excluded, so that only hydrogen permeation through the separator is evaluated.

Furthermore, Fig. 4 also shows the results of the reference measurements. It can be seen for both technologies that the determined crossover fluxes remain constant with increasing current density and that the values are small compared to the results during electrolysis operation. These constant measurement values can be explained by the fact that the electrolyte is gas saturated by the continuous supply of hydrogen and oxygen, which results in a constant diffusive flux across the separating unit (s. Eq. 15), whereas no other crossover mechanisms occur as the experiments were conducted under atmospheric pressure conditions and no supersaturation can be formed. Additionally, Fig. 4 provides values for the purely diffusive hydrogen crossover at zero current, which are represented by hollow symbols. For the PEM electrolysis experiments these values were determined according to the aforementioned pressure drop method, whereas the values for the alkaline system were calculated from data provided by Schalenbach et al.[24] Here it is recognizable that the reference measurements of both electrolysis systems show excellent agreement with the zero current values of the pressure drop and literature data at atmospheric pressure, which therefore confirms the purely diffusive crossover occurring in these measurements.

In contrast to the data of the reference measurements, the results of both technologies show that hydrogen crossover through the separating unit primarily increases with rising current density and also system pressure during electrolysis operation.

Thus, Fig. 4a reveals a clear linear dependency of the hydrogen crossover on the current density for the PEM electrolysis measurements, which has also been observed in the literature, e.g. Refs. 5 and 14. This linear growth can be explained with mass transport resistances within the cathode catalyst layer that cause an increasing supersaturation of dissolved hydrogen with increasing current density.[5] The slope of the crossover is approximately equal for all the investigated pressure stages, since the mass transport resistance is assumed to be mainly affected by geometrical and/or structural parameters and less by operating conditions.[5,13] As the linear extension of the determined hydrogen crossover matches the zero current values excellently, a linear dependency of the hydrogen crossover is also assumed for even smaller current densities. Finally, it can also be seen that the balanced and differential pressure operation at a system or cathodic pressure of 10 bar show no significant difference in hydrogen crossover. This was expected, since literature also suggests no pressure-driven convective crossover for Nafion membranes at this pressure gradient.[23,41]

The AEL results are shown in Fig. 4b, where no specific trend becomes obvious at first. However, the data suggests that hydrogen crossover initially also increases with rising current density until a plateau is formed. Additionally, increasing system pressures seem to shift the formation of the plateau toward higher current densities. This effect may be explained with an increase of the hydrogen mass transfer coefficient from the liquid electrolyte into the gas phase at higher current densities. As previously mentioned, electrolysis products are assumed to be generated in dissolved form before gas is evolved in a subsequent physical step. Therefore, dissolved hydrogen may leave the electrode either in gaseous state through the transport into adhering bubbles and subsequent bubble detachment or in dissolved form through transport into the electrolyte bulk or across the separator. For the description of this phenomenon Vogt[56] introduced the gas evolution efficiency, which describes the ratio of product transported into gas bubbles at the electrode to the total generated flux. Literature values for the gas evolution efficiency[57–59] show a strong increase at low current densities (up to approx. 0.2 A cm^{-2}) until a linear dependency can be observed. Hence, at very small current densities nearly the total amount of product leaves the electrode in dissolved form. As the current density increases, the concentration of dissolved hydrogen becomes high enough to activate nucleation sites, which enable the evolution of gas bubbles at the electrode.[50] Therefore, the fraction of product leaving the electrode in dissolved form decreases with higher current densities, which consequently limits the flux of dissolved hydrogen across the separator. Furthermore, it is assumed that an increase in pressure moves the gas evolution efficiency toward higher current densities, which would explain the later plateau formation. Thus, a pressure increase enhances the mandatory dissolved gas concentration for activation of nucleation sites and reduces the mass transfer coefficient ($k_L = f(Re)$) of dissolved hydrogen into adhering bubbles, as the Reynolds number $Re = u \cdot d_b/\nu$ is decreased by

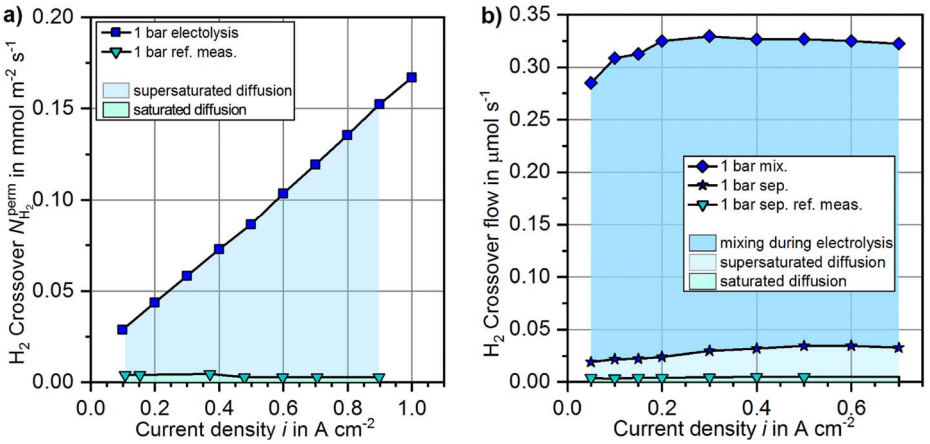

Figure 5. Crossover breakdown for the PEM (a) and classical alkaline (b) electrolysis experiments under atmospheric pressure conditions. Since crossover through electrolyte mixing does not represent a cell-specific quantity, the y-axis of the alkaline experiments shows the actual molar flow rates.

smaller bubble diameters. Of course, it may also be possible that the determined crossover is superimposed by the convective transport of dissolved hydrogen across the separator. However, this is questioned with the current state of knowledge as the anodic cycle showed an approximately 20 mbar higher pressure at elevated pressure stages, which would have suppressed convective hydrogen permeation. Finally, in contrast to PEM electrolysis, where a linear dependency of the crossover can be assumed for the complete investigated current density range, the analysis of the alkaline zero current values suggests a strong increase of the crossover at small current densities. However, further investigations are necessary to confirm this presumption.

The overall comparison of the electrolysis results shows that diffusive crossover in PEM electrolysis is more than one order of magnitude higher than in AEL, which is mainly a consequence of the lower hydrogen solubility in concentrated potassium hydroxide solution. So, in comparison to pure water the solubility is decreased by a factor of 8 in 30 wt% KOH at a temperature of 30°C and a gas partial pressure of 1.013 bar.[7] Similar information was published by Schalenbach et al.,[60] who reported a 38 times lower hydrogen permeability coefficient in Zirfon soaked with 30 wt% KOH compared to Nafion 117 immersed in water at a cell temperature of 80°C.

Crossover breakdown.—In this chapter the respective share of the different crossover mechanisms is graphically depicted in Fig. 5 for PEM and classical alkaline water electrolysis with mixed electrolyte cycles at atmospheric pressure conditions.

Fig. 5a shows the breakdown of the achieved PEM electrolysis results. Here, the hydrogen crossover can be divided into two different areas. Firstly, a small proportion of the overall crossover is caused by diffusion due to saturated dissolved hydrogen, which has been determined with the reference measurements. The second and major part is also a result of diffusion, but is caused by a supersaturated hydrogen concentration in the cathodic half cell. The percentage of this effect increases with current density. Whereas 86% are transported across the membrane at 0.1 A cm^{-2}, a current density of 1 A cm^{-2} shows a share of 98% since supersaturation increases linearly with current density as it was stated before.

Furthermore, the results indicate that the percentage of crossover due to supersaturation decreases with increasing cathodic pressure. The values for the higher cathodic pressures are based on the results of the pressure drop method. At a pressure of 10 bar the share is 70%, while only 53% are determined at 20 bar for a current density of 1 A cm^{-2}. This can be explained by the fact that diffusive crossover due to saturated dissolved hydrogen increases with raising pressure, whereas the supersaturation is nearly pressure independent. Thus, the current density effect loses importance at very high cathodic pressures.

The crossover breakdown for the atmospheric AEL experiments is shown in Fig. 5b. Since the classical process management with mixed electrolyte cycles is chosen for the evaluation of the individual crossover fractions, the previously shown area-related diffusive crossover fluxes need to be multiplied by the surface area of the separator as crossover by mixing the electrolyte cycles does not represent a cell-, but electrolyzer-specific value.

Therefore, Eq. 9 is used for the estimation of the overall crossover with mixed electrolyte cycles and then multiplied by the surface area of the separator. In order to simplify the evaluation, it is assumed that the diffusive crossover due to electrolyte saturation and supersaturation, which were determined with separated cycles, can also be transferred to mixed electrolyte cycles. However, the diffusive crossover should be slightly smaller with mixed electrolyte cycles, since the electrolyte entering the half cells is already saturated with hydrogen and oxygen, thus reducing the concentration gradient across the separator. Therefore, the share of crossover due to electrolyte mixing might be even larger for this specific test station than shown in the following. The trend of the diffusive crossover due to saturation and supersaturation of the electrolyte was already discussed in the previous section. At a current density of 0.7 A cm^{-2} their shares amount to 1.4% and 8.6%, respectively. Here, similar to PEM electrolysis, a slight increase of the diffusional crossover due to supersaturation can be observed with rising current density as the share at 0.1 A cm^{-2} is determined to be 6.0%.

However, it is obvious that the mixing of the electrolyte cycles represents the largest source for transferring hydrogen into the anodic half cell. This crossover flow remains approximately constant over the whole investigated current density range as regardless of the applied current density gas-saturated electrolyte is always fed into the half cells. Only at smaller current densities a minor increase of this mechanism is recognizable, which might be regarded to not only dissolved species, but also gas bubbles being transported back into the electrolysis cell. The percentage of crossover due to electrolyte mixing is the highest for all investigated pressure stages, yielding 90% at atmospheric pressure, 88% at 10 bar and 95% at 20 bar for a current density of 0.7 A cm^{-2}. These high values exemplify once more that an improvement of the anodic hydrogen concentration can in particular be achieved by an optimized lye circulation strategy.

Variation of separating unit thickness.—The experimental results showed that safety issues can limit the operating ranges of the electrolyzers under certain conditions with the investigated state-of-the-art separating unit materials. In the following section, the influence of the separating unit thickness on the anodic hydrogen content is studied. Therefore, the anodic gas contamination is estimated for thinner separating units on basis of the obtained experimental data.

It is assumed for the PEM system that neither supersaturation nor the permeability coefficient are influenced by the membrane thickness. Thus, the overall crossover flux $N_{H_2}^{cross}$ for different membrane thicknesses can be calculated according to Eq. 22.

$$N_{H_2,PEM}^{cross} = N_{H_2,exp}^{perm} \frac{\delta_{N117}}{\delta_{sep}} \quad [22]$$

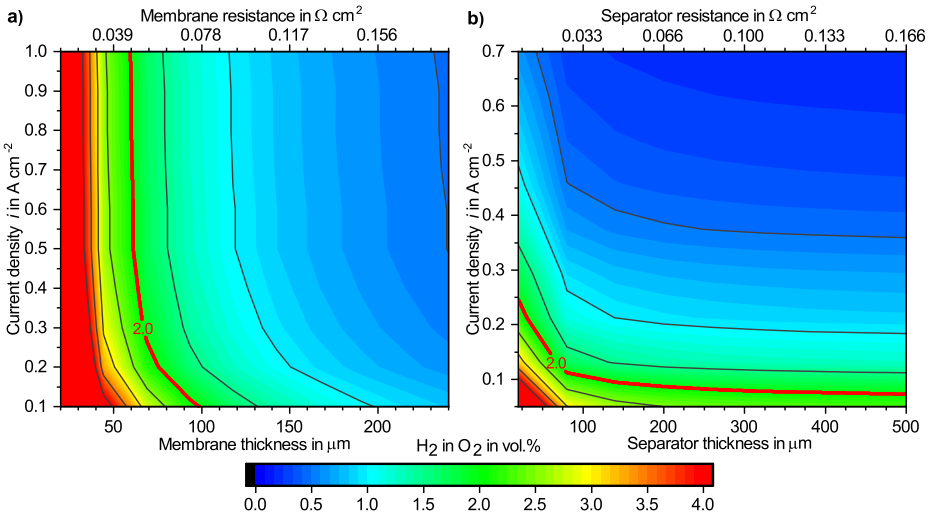

Figure 6. Anodic hydrogen content as a function of separating unit thickness and current density for PEM (a) and alkaline electrolysis (b) at atmospheric pressure, a temperature of 60°C and 32 wt% KOH. Calculations are based on the obtained experimental data for the N117 membrane and the Zirfon separator.

The same assumptions also apply for the alkaline system. Furthermore, crossover through electrolyte mixing is also independent on separator thickness. Therefore, Eq. 23 may be used for the calculation of the overall crossover flux at alternative separator thicknesses.

$$N^{\text{cross}}_{\text{H}_2,\text{AEL}} = N^{\text{mix}}_{\text{H}_2,\text{exp}} + N^{\text{perm}}_{\text{H}_2,\text{exp}} \frac{\delta_{\text{Zirfon}}}{\delta_{\text{sep}}} \quad [23]$$

Subsequently, the hydrogen content can be calculated with Eq. 6 for both technologies in variation of the separating unit thickness. The obtained results are depicted in Fig. 6 for atmospheric pressure conditions and a temperature of 60°C. The ohmic resistances R_{sep} shown there are calculated according to Eq. 24.

$$R_{\text{sep}} = \frac{\delta_{\text{sep}}}{\sigma_{\text{sep}}} \quad [24]$$

Here, σ_{sep} denotes the ionic conductivity of the separating units, which were achieved from the literature. For a Nafion 117 membrane immersed in water the conductivity is given with roughly 13.5 S m^{-1} at 60°C.[61] Vermeiren et al.[62] provide a value of 0.166 Ω cm^2 for a Zirfon separator with a thickness of 500 µm at a temperature of 60°C and a potassium hydroxide concentration of 30 wt%. Correspondingly, the insertion into Eq. 24 yields an ionic conductivity of 30.1 S m^{-1}. Although the electrolyte applied in this study is slightly higher concentrated, the value of Vermeiren et al. can still give an approximate estimation.

The heatmaps of Fig. 6 show the correlation between the separating unit thickness on the bottom or the respective electrical resistance on the top x-axis and current density on the y-axis. The hydrogen content itself is depicted in form of contour lines. A comparison of the two technologies shows that the contour lines point in different directions. Thus, in PEM electrolysis the lines are ordered vertically, while the hydrogen content in AEL roughly shows a horizontal curve.

The contour plot for PEM electrolysis reveals that the hydrogen content strongly increases with a decreasing membrane thickness. This results from the purely diffusive character of hydrogen crossover in the PEM setup, which increases inversely proportional with a decreasing membrane thickness (s. Eq. 10). Consequently, the trend toward thinner membranes to reduce ohmic losses can only be realized with a simultaneous reduction of the hydrogen content in the anode or the crossover itself.

Fig. 6b shows a totally different trend for the hydrogen content with a decreasing separator thickness in AEL. Here, the hydrogen content is nearly independent on the separator thickness. An increase of the hydrogen concentration due to diffusion can only be observed at thicknesses below 100 µm. This can be explained with the fact that the main portion of hydrogen crossover is caused by mixing of the electrolyte cycles, whereas diffusive crossover only represents a very small share. So, the alkaline cell, equipped with a Zirfon separator, shows that the reduction of the separator thickness offers high potential for improving ohmic losses if the mechanical stability can be maintained and this is technically feasible. However, it has to be said that convective crossover gains in importance with a decreasing separator thickness, which necessitates a complex pressure control to keep the differential pressure at a minimum.

Mitigation Strategies

In this section strategies for the mitigation of crossover and corresponding side effects are discussed for both technologies. These strategies are summarized in Table II and divided into five categories. The different strategies are evaluated regarding the five following criteria: safety issues (H_2 in O_2), degradation (catalyst layer/electrode, membrane) due to crossover, Faraday efficiency, electrochemical performance and costs.

Separating unit.—Particularly in PEM electrolysis the use of highly ion-conductive membranes with lower hydrogen permeability is an interesting possibility to solve existing safety issues. This may not only increase the Faraday efficiency, but the overall performance of the electrolyzer. In literature some promising candidates can be found, e.g. radiation grafted membranes[63] or hydrocarbon-based materials.[64] In contrast, for AEL the previous results suggest that diffusive crossover may not be significantly reduced with advanced materials, as the diffusional flux is already very limited due to the poor solubility of hydrogen and oxygen in the highly concentrated electrolyte. However, if lower electrolyte concentrations are to be used in the future, this approach will become more important as better cell efficiencies can be achieved with ion-conductive membranes in this operating regime, e.g. Refs. 65 and 66.

Another possibility for a reduction of the anodic hydrogen content would be the increase of the membrane thickness, which of course would be linked to a reduction of the electrolyzer performance. So, this is not a real option and also does not reflect the trend of research and development.

Recombination catalyst.—A totally different approach is the application of recombination catalysts, which enable the reaction of permeated hydrogen back to water. For PEM electrolysis, it has already been shown that the incorporation of platinum is able to reduce the anodic hydrogen content significantly if the catalyst is applied to the back side of the current collectors. Even better results were obtained, when the recombiner was positioned downstream of the gas separators as the optimal operation necessitates dry gases.[8] Additionally, it is also conceivable to integrate the catalyst directly into the electrode[9] or separating unit in order to provide a large contact area

Table II. Approaches for crossover reduction and negative consequences in PEM (left)/AEL (right). Meaning of the symbols: ++ very effective, + good, o no effect or slightly positive/negative, - negative, - - very negative, ? effect cannot be estimated.

	H_2 in O_2 (safety)	Degradation	Faraday	Performance	Cost
1. Separating unit					
a) advanced materials with high ionic conductivity and low permeability[63,64]	+/o	?/?	+/o	++/+	?/?
b) thicker separating units	+/o	+/o	+/o	- -/- -	-/-
2. Recombination catalyst					
a) external recombination[8]	+/+	o/o	o/o	o/o	-/-
b) on the backing layers [8] (PTL, bipolar plate)	+/+	o/o	o/o	o/o	-/-
c) within the catalyst layer/electrode[9]	++/+	?/?	?/o	o/o	-/-
d) within the membrane/separator	+/+	?/o	o/o	-/o	-/-
3. Supersaturation					
a) improved catalyst layers/electrodes, less transport resistances	++/+	+/o	+/+	++/++	o/o
b) ultrasonic field[67]	+/+	?/?	+/+	+/+	- -/- -
c) magnetic field[51,68,73–76]	+/?	?/?	+/?	+/+	- -/- -
d) super gravity field[69,77]	?/?	?/?	?/?	+/+	- -/- -
4. Interlayer					
a) thin layers/sheets that are capable for the ionic transport, but gas-tight[70,71]	++/o	+/o	++/o	?/o	-/-
b) 3rd/4th electrode[72]	++/+	?/?	+/+	-/-	- -/- -
5. Process management (only AEL)					
a) advanced gas/liquid separators	/+	/o	/+	/o	/-
b) mixing strategies[7,55]	/++	/o	/+	/o	/o
c) advanced mixing appliances	/++	/o	/++	/o	/- -

between the permeating gases and the recombination catalyst. But it is important to emphasize that the introduction of recombination catalysts only reduces the risk of explosive mixtures, whereas the Faraday efficiency is not improved as this measure does not address the origin of crossover.

Reduction of supersaturation.—As it was discussed before, supersaturation strongly enhances the diffusional crossover in both technologies. Therefore, especially when membrane electrode assemblies are applied, it should be examined whether transport resistances that contribute to the formation of supersaturation can be reduced by improved geometrical and structural properties of the electrodes or catalyst layers. The comparison of literature data for PEM electrolysis reveals different slopes for the crossover increase with rising current density, which is presumed to be mainly an effect of different geometrical or structural properties.[5]

Furthermore, the influence of external impacts on the electrolysis cell on supersaturation of the electrolyte could be investigated. Li et al.[67] reported that they were able to reduce the energy demand in AEL, when the cell was operated under the influence of ultrasound as the evolving gas bubbles were removed from the electrode surface more quickly. Here, it is also conceivable that an ultrasonic field could promote the formation of gas bubbles from the supersaturated electrolyte, which consequently would reduce the dissolved concentration of electrolysis products. Similar approaches are the application of magnetic[68] or gravitational[69] fields, which have already been shown to reduce cell voltage in AEL. It is difficult to estimate in which way these technologies influence supersaturation of dissolved gas within the respective electrolysis technology, but certainly represent an interesting field of research, since performance, crossover and also Faraday efficiency could be improved.

Interlayer.—Another option to reduce crossover or the corresponding negative effects is placing thin interlayers within the separator or between the electrode and the separating unit. These interlayers could consist of a material that is characterized by a low permeability coefficient, but capable for the ionic transport. For instance, this approach was shown using hexagonal boron nitride and graphene in methanol fuel cells, e.g. Ref. 70. For PEM fuel cells this was also successfully demonstrated through the application of a graphene oxide/cerium oxide interlayer.[71] This method could be very effective, because of the reduction of crossover at its origin and therefore all negative effects.

Another interlayer could be realized in form of a third electrode that is electrically connected to the hydrogen evolving cathode and supplied by an additional power source. In case of PEM water electrolysis the permeating hydrogen can be oxidized to protons at the third electrode, which will then be pumped back to the cathode electrochemically. This method was already successfully demonstrated by Schalenbach et al.[72] They also showed that this third electrode can work in combination with the oxygen evolving anode. In this case permeating hydrogen is oxized at the additional electrode, while the anode works as a fuel cell locally. Furthermore, a four electrode arrangement supplied by two additional power sources could also be used to send back permeating hydrogen and oxygen in AEL. Here, one electrode each would have to be connected to the anode and cathode of the electrolysis cell, whereby the reverse reactions of the corresponding gas-evolving electrode would then take place there. However, placing additional electrodes is expensive and further complicates cell stack design.

Finally, it is also possible to apply a recombination catalyst as an interlayer, which has already been described before (s. Table II 2.d).

Process management.—It could be shown for AEL that mixing of the electrolyte cycles represents the most important crossover mechanism. For this reason advanced gas separators should ensure that no gaseous species are transported back into the cell even at high system pressures.

Furthermore, Schug[55] reported that the amount of recycled dissolved species can be reduced with an adequate electrolyte circulation control. Here, the recirculation rate should be chosen as low as possible to minimize the convective crossover of electrolysis products through mixing anolyte and catholyte. Furthermore, this crossover mechanism loses importance with a growing electrolysis plant size or electrode area as the gas production rate is increased, whereas the amount of recycled species stays equal at identical electrolyte flow rates.

Additionally, it could be demonstrated before[7] that periodic switching between mixed and separated cycles is capable of reducing the mean anodic hydrogen content while maintaining an equal electrolyte concentration in the anolyte and catholyte. It may also be conceivable that electrolysis is carried out with separated cycles under part-load operation, whereas a merging of the cycles is initiated as soon as a specific minimum current density is exceeded.

Eventually an advanced mixing appliance is proposed in Table II. This could be realized by an additional electrolyte mixing tank equipped with an ion-exchange membrane that still enables an equalization of the anodic and cathodic electrolyte concentration. Consequently, the transport of cycled gas bubbles could be prevented.

Furthermore, crossover due to the transport of dissolved species into the opposite half cell can be reduced in comparison to the direct mixing of anolyte and catholyte as the applied membrane serves as an additional diffusion barrier.

Conclusions

This study provides a summary of the crossover mechanisms occurring in PEM and alkaline water electrolysis and experimentally investigates the influence of current density, system pressure and various process management strategies on the resulting gas purity. In addition, reference measurements for the determination of purely diffusive crossover in both technologies are conducted. For a fair comparison of the two technologies, a uniform operating temperature of 60°C and state-of-the-art separating unit materials, Nafion 117 in PEM and Zirfon in alkaline electrolysis, were chosen.

Generally the results of both technologies indicate that the anodic gas contamination increases significantly with decreasing current density and rising system pressure, which is mainly a consequence of increased dissolved gas concentration at elevated pressures. In fact, under specific operating conditions the determined hydrogen concentrations even exceeded 2 vol.% in the anodic product gas stream, so that a safe plant operation was no longer possible. Here, the comparison of different process management strategies in AEL showed that the anodic hydrogen concentration is particularly influenced by mixing anolyte and catholyte, since a safe operation of the electrolyzer with separated cycles could be ensured at all investigated system pressures. Furthermore, the PEM experiments revealed that no distinction in the anodic hydrogen concentration is recognizable between balanced and differential pressure operation at an applied pressure gradient of 10 bar.

In a subsequent step the measured anodic hydrogen concentrations of both technologies were converted into permeation fluxes to illustrate the influence of current density and system pressure more clearly. As a result a linear increase of hydrogen permeation toward rising current densities could be observed in PEM electrolysis at all pressure levels. It is assumed that this linear growth is caused by a supersaturation of dissolved hydrogen, which is caused by mass transport resistances within the cathode catalyst layer. The supersaturation increases with current density, thus enhancing the diffusive permeation across the membrane. In comparison to the reference measurements, which showed no current density dependence of permeating hydrogen, supersaturation multiplied the diffusive crossover by a factor of 20 at a current density of 1 A cm^{-2} and a system pressure of 1 bar. However, the influence of supersaturation is seen to decrease with increasing system pressure. While the share on the overall crossover flux amounts to 98% at 1 A cm^{-2} and 1 bar, only 53% are determined at a pressure of 20 bar.

In contrast, the hydrogen permeation data of the alkaline experiments did not show such a clear dependency on the current density. However, it is observed at all investigated pressure stages that hydrogen crossover initially also increases with rising current density until a maximum permeation flux is reached. Similarly to PEM electrolysis it is assumed that the diffusive crossover is enhanced by a supersaturated electrolyte. But this effect is presumed to lose influence at higher current densities as a greater proportion of evolved hydrogen is directly transported into gas bubbles adhering to the electrode, which consequently limits the diffusive crossover flux. Electrolyte mixing represents the most influential crossover mechanism with a share of 90% under atmospheric pressure conditions and a current density of 0.7 A cm^{-2}. Consequently diffusion due to saturation and supersaturation only yields 1.4% and 8.6% for this experimental setup.

Overall, PEM electrolysis showed a more than one order of magnitude higher diffusive crossover flux than AEL, which is particularly a consequence of the significantly lower hydrogen solubility in concentrated potassium hydroxide solution. Therefore, this study also provides an estimation of the influence of the separating unit thickness on the expected anodic gas contamination. Due to the inversely proportional dependency of the hydrogen crossover on the membrane thickness, a strong increase of the anodic hydrogen contamination is evident with decreasing membrane thicknesses in PEM electrolysis. Contrarily, the estimation shows a huge optimization potential for a reduction of the separator thickness in AEL as no meaningful increase of the anodic hydrogen concentration is observable down to thicknesses of 100 μm as crossover is mainly influenced by electrolyte mixing.

Finally, this study provides a summary of possible mitigation strategies that could help to reduce hydrogen crossover or at least the anodic foreign gas content. To this end, literature references are mentioned in which initial investigations have already been reported.

Acknowledgments

The authors gratefully acknowledge the financial support by the Federal Ministry of Education and Research of Germany in the framework of PowerMEE (project number 03SF0536B) and the DFG in the framework of the projects INST 189/182-1 FUGG and TU 89/18-1.

List of Symbols

a	specific surface area	m^{-1}
A_{el}	cross-sectional electrode area	m^2
A_{sep}	cross-sectional separating unit area	m^2
c_{H_2}	dissolved hydrogen concentration	mol m^{-3}
c_{solv}	concentration of solvent within separating unit	mol m^{-3}
d	pore diameter of separating unit	m
d_b	gas bubble diameter	m
D_{H_2}	diffusion coefficient of dissolved hydrogen in solvent	$m^2 s^{-1}$
F	Faraday constant	96485A s mol^{-1}
i	current density	A m^{-2}
k_L	mass transfer coefficient	m s^{-1}
K_{H_2}	hydrogen permeability coefficient	mol Pa^{-1} m^{-1} s^{-1}
K_{koz}	Kozeny constant	–
K_{sep}	hydraulic permeability	m^2
n_{drag}	drag coefficient	–
N_{H_2}	hydrogen flux	mol m^{-2} s^{-1}
N_{O_2}	oxygen flux	mol m^{-2} s^{-1}
p	absolute pressure	Pa
p_i	partial pressure of comp. i	Pa
R_{sep}	ohmic resistance of separating unit	Ω cm^2
Re	Reynolds number	–
S_{H_2}	solubility of hydrogen in solvent	mol Pa^{-1}m^{-3}
T	temperature	K
u	velocity	m s^{-1}
v_{solv}	hydraulic velocity of solvent	m s^{-1}
$\dot{V}$	volumetric flow rate of electrolyte	$m^3 s^{-1}$

Greek

δ_{sep}	separating unit thickness	m
ε	porosity	–
η	dynamic viscosity of solvent	Pa s
ν	kinematic viscosity of solvent	$m^2 s^{-1}$
σ_{sep}	ionic conductivity	S m^{-1}
τ	tortuosity	–
Φ_{H_2}	anodic hydrogen fraction	–

Subscripts/Superscripts

ano	anode
cat	cathode
conv	convective
cross	crossover
diff	diffusive
dp	differential pressure
drag	drag
eff	effective
mix	electrolyte mixing
perm	permeation
sep	separator
solv	solvent

ORCID

B. Bensmann http://orcid.org/0000-0001-8685-7192

References

1. L. M. Gandia, R. Oroz, A. Ursua, P. Sanchis, and P. M. Dieguez, *Energ. Fuel.*, **21**(3), 1699 (2007).
2. R. E. Clarke, S. Giddey, and S. P. S. Badwal, *Int. J. Hydrogen Energ.*, **35**(3), 928 (2010).
3. M. Carmo, D. L. Fritz, J. Mergel, and D. Stolten, *Int. J. Hydrogen Energ.*, **38**(12), 4901 (2013).
4. S. A. Grigoriev, V. I. Porembskiy, S. V. Korobtsev, V. N. Fateev, F. Auprête, and P. Millet, *Int. J. Hydrogen Energ.*, **36**(3), 2721 (2011).
5. P. Trinke, B. Bensmann, and R. Hanke-Rauschenbach, *Int. J. Hydrogen Energ.*, **42**(21), 14355 (2017).
6. W. Hug, J. Divisek, J. Mergel, W. Seeger, and H. Steeb, *Int. J. Hydrogen Energ.*, **17**(9), 699 (1992).
7. P. Haug, M. Koj, and T. Turek, *Int. J. Hydrogen Energ.*, **42**(15), 9406 (2017).
8. S. A. Grigoriev, P. Millet, S. V. Korobtsev, V. I. Porembskiy, M. Pepic, C. Etievant, C. Puyenchet, and V. N. Fateev, *Int. J. Hydrogen Energ.*, **34**(14), 5986 (2009).
9. H. Ito, N. Miyazaki, M. Ishida, and A. Nakano, *Int. J. Hydrogen Energ.*, **41**(45), 20439 (2016).
10. M. Inaba, T. Kinumoto, M. Kiriake, R. Umebayashi, A. Tasaka, and Z. Ogumi, *Electrochim. Acta*, **51**(26), 5746 (2006).
11. M. Chandesris, V. Médeau, N. Guillet, S. Chelghoum, D. Thoby, and F. Fouda-Onana, *Int. J. Hydrogen Energ.*, **40**(3), 1353 (2015).
12. M. Schalenbach, *Int. J. Hydrogen Energ.*, **41**(1), 729 (2016).
13. P. Trinke, B. Bensmann, and R. Hanke-Rauschenbach, *Electrochem. Commun.*, **82**, 98 (2017).
14. S. Al Shakhshir, X. Cui, S. Frensch, and S. K. Kær, *Int. J. Hydrogen Energ.*, **42**(34), 21597 (2017).
15. A. Manabe, H. Domon, J. Kosaka, T. Hashimoto, T. Okajima, and T. Ohsaka, *J. Electrochem. Soc.*, **163**(11), 3139 (2016).
16. P. Haug, B. Kreitz, M. Koj, and T. Turek, *Int. J. Hydrogen Energ.*, **42**(24), 15689 (2017).
17. Q. Duan, H. Wang, and J. Benziger, *J. Membrane Sci.*, **392-393**, 88 (2012).
18. Brochure Zirfon Perl UTP 500, https://www.agfa.com/sp/global/en/binaries/ZirfonPerl_UTP500_tcm611-56748.pdf, Accessed: 2018-01-15.
19. T. Sakai, H. Takenada, N. Wakabayashi, Y. Kawami, and E. Torikai, *J. Phys. Chem.-US*, **132**(6), 1328 (1985).
20. M. K. Tham, R. D. Walker, and K. E. Gubbins, *J. Phys. Chem.-US*, **74**(8), 1747 (1970).
21. B. Bensmann, R. Hanke-Rauschenbach, and K. Sundmacher, *Int. J. Hydrogen Energ.*, **39**(1), 49 (2014).
22. T. Sakai, H. Takenaka, and E. Torikai, *J. Electrochem. Soc.*, **133**(1), 88 (1986).
23. M. Schalenbach, T. Hoefner, P. Paciok, M. Carmo, W. Lueke, and D. Stolten, *J. Phys. Chem. C*, **119**(45), 25145 (2015).
24. M. Schalenbach, W. Lueke, and D. Stolten, *J. Electrochem. Soc.*, **163**(14), 1480 (2016).
25. F. Marangio, M. Santarelli, and M. Cali, *Int. J. Hydrogen Energ.*, **34**(3), 1143 (2009).
26. M. Schalenbach, M. Carmo, D. L. Fritz, J. Mergel, and D. Stolten, *Int. J. Hydrogen Energ.*, **38**(35), 14921 (2013).
27. H. Kim, M. Park, and K. S. Lee, *Int. J. Hydrogen Energ.*, **38**(6), 2596 (2013).
28. P. Trinke, B. Bensmann, S. Reichstein, R. Hanke-Rauschenbach, and K. Sundmacher, *J. Electrochem. Soc.*, **163**(11), 3164 (2016).
29. J. Fimrite, B. Carnes, H. Struchtrup, and N. Djilali, *J. Electrochem. Soc.*, **152**(9), 1815 (2005).
30. R. B. Evans and G. M. Watson, *J. Chem. Phys.*, **35**(6), 2076 (1961).
31. C. L. Young, *Hydrogen and deuterium, Solubility data series, 5/6.*, Pergamon Press, 1981.
32. R. Wiebe and V. L. Gaddy, *J. Am. Chem. Soc.*, **56**(1), 76 (1934).
33. P. Ruetschi and R. F. Amlie, *J. Phys. Chem.-US*, **70**(3), 718 (1966).
34. M. B. Knaster and L. A. Apel'baum, *Russ. J. Phys. Ch.*, **38**, 120 (1964).
35. D. R. Stull, *Ind. Eng. Chem.*, **39**(4), 517 (1947).
36. J. Balej, *Int. J. Hydrogen Energ.*, **10**(4), 233 (1985).
37. P. Medina and M. Santarelli, *Int. J. Hydrogen Energ.*, **35**(11), 5173 (2010).
38. M. Mulder, Characterisation of membranes, in: M. Mulder (Ed.), *Basic Principles of Membrane Technology*, Springer Netherlands, Dordrecht, pp. 157–209 1996.
39. T. Ozgumus, M. Mobedi, and U. Ozkol, *Eng. Appl. Comp. Fluid*, **8**(2), 308 (2014).
40. M. Schalenbach, *J. Electrochem. Soc.*, **164**(14), X23 (2017).
41. F. Barbir, *Sol. Energy*, **78**(5), 661 (2005).
42. B. Bensmann, R. Hanke-Rauschenbach, I. K. Peña Arias, and K. Sundmacher, *Electrochim. Acta*, **110**, 570 (2013).
43. B. Bensmann, R. Hanke-Rauschenbach, G. Müller-Syring, M. Henel, and K. Sundmacher, *Appl. Energ.*, **167**, 107 (2016).
44. S. A. Grigoriev, A. A. Kalinnikov, P. Millet, V. I. Porembskiy, and V. N. Fateev, *J. Appl. Electrochem.*, **40**(5), 921 (2010).
45. L. C. Jacobson, X. Ren, and V. Molinero, *J. Phys. Chem. C*, **118**(4), 2093 (2014).
46. K. Onda, T. Murakami, T. Hikosaka, M. Kobayashi, R. Notu, and K. Ito, *J. Electrochem. Soc.*, **149**(8), 1069 (2002).
47. V. Schroeder, B. Emonts, H. Janssen, and H.-P. Schulze, *Chem. Eng. Technol.*, **27**(8), 847 (2004).
48. J. Eigeldinger and H. Vogt, *Electrochim. Acta*, **45**(27), 4449 (2000).
49. R. J. Balzer and H. Vogt, *J. Electrochem. Soc.*, **150**(1), 11 (2003).
50. H. Vogt, K. Kreysa, S. Vasudevan, R. Wüthrich, J. D. Abou Ziki, and R. El-Haddad, *Electrochemical reactors*, Ullmann's encyclopedia of industrial chemistry, Wiley-VCH, 2013.
51. H. Matsushima, D. Kiuchi, and Y. Fukunaka, *Electrochim. Acta*, **54**(24), 5858 (2009).
52. K. Kikuchi, H. Takeda, B. Rabolt, T. Okaya, Z. Ogumi, Y. Saihara, and H. Noguchi, *J. Electroanal. Chem.*, **506**(1), 22 (2001).
53. H. Vogt, *Electrochim. Acta*, **56**(3), 1409 (2011).
54. R. T. Ferrell and D. M. Himmelblau, *AIChE J.*, **13**(4), 702 (1967).
55. C. A. Schug, *Int. J. Hydrogen Energ.*, **23**(12), 1113 (1998).
56. H. Vogt, *Electrochim. Acta*, **29**(2), 167 (1984).
57. H. Vogt, *Electrochim. Acta*, **30**(2), 265 (1985).
58. J. M. Chin Kwie Joe, L. J. J. Janssen, S. J. D. van Strelen, J. H. G. Verbunt, and W. M. Sluyter, *Electrochim. Acta*, **33**(6), 769 (1988).
59. J. St-Pierre, N. Massé, and M. Bargeron, *Electrochim. Acta*, **40**(8), 1013 (1995).
60. M. Schalenbach, G. Tjarks, M. Carmo, W. Lueke, M. Mueller, and D. Stolten, *J. Electrochem. Soc.*, **163**(11), 3197 (2016).
61. H. Ito, T. Maeda, A. Nakano, and H. Takenaka, *Int. J. Hydrogen Energ.*, **36**(17), 10527 (2011).
62. P. Vermeiren, W. Adriansens, J. Moreels, and R. Leysen, *Int. J. Hydrogen Energ.*, **23**(5), 321 (1998).
63. A. Albert, A. O. Barnett, M. S. Thomassen, T. J. Schmidt, and L. Gubler, *ACS Appl. Mater. Inter.*, **7**(40), 22203 (2015).
64. C. K. Mittelsteadt and J. A. Staser, *Electrolyzer membranes, in: Polymer Science: A Comprehensive Reference*, Elsevier, 2012, pp. 849–871.
65. L. A. Diaz, J. Hnat, N. Heredia, M. M. Bruno, F. A. Viva, M. Paidar, H. R. Corti, K. Bouzek, and G. C. Abuin, *J. Power Sources*, **312**, 128 (2016).
66. M. R. Kraglund, D. Aili, K. Jankova, En. Christensen, Q. Li, and J. O. Jensen, *J. Electrochem. Soc.*, **163**(11), 3125 (2016).
67. S. Li, C. Wang, and C. Chen, *Electrochim. Acta*, **54**(15), 3877 (2009).
68. M. Lin, L. Hourng, and C. Kuo, *Int. J. Hydrogen Energ.*, **37**(2), 1311(2012).
69. M. Wang, Z. Wang, and Z. Guo, *Int. J. Hydrogen Energ.*, **35**(8), 3198 (2010).
70. S. M. Holmes, P. Balakrishnan, V. S. Kalangi, X. Zhang, M. Lozada-Hidalgo, P. M. Ajayan, and R. R. Nair, *Adv. Energy Mater.*, **7**(5), 1601216 (2017).
71. M. Breitwieser, T. Bayer, A. Büchler, R. Zengerle, S. M. Lyth, and S. Thiele, *J. Power Sources*, **351**, 145 (2017).
72. M. Schalenbach and D. Stolten, *Electrochim. Acta*, **156**, 321 (2015).
73. H.-B. Lee, J.-C. Tsau, and C.-Y. Lee, *J. Nanomater.*, **2013**(11), 1 (2013).
74. H. Matsushima, T. Iida, and Y. Fukunaka, *Electrochim. Acta*, **100**, 261 (2013).
75. D. Baczyzmalski, F. Karnbach, X. Yang, G. Mutschke, M. Uhlemann, K. Eckert, and C. Cierpka, *J. Electrochem. Soc.*, **163**(9), E248 (2016).
76. L. Elias and A. Chitharanjan Hegde, *Electrocatalysis*, **8**(4), 375 (2017).
77. H. Matsushima, D. Kiuchi, Y. Fukunaka, and K. Kuribayashi, *Electrochem. Commun.*, **11**(8), 1721 (2009).